

COMPARISON OF LATTICE DISCRETE PARTICLE MODEL (LDPM) IMPLEMENTATIONS: LESSONS LEARNED AND FUTURE WORK

EROL LALE*, KE YU* MATTHEW TROEMNER[†], MADURA PATHIRAGE[‡], GILLES
PIJAUDIER-CABOT[∨], JULIEN KHOURY[∨], IOANNIS KOUTROMANOS*, JAN ELIAS[^],
MONIKA STREDULOVA[^], TIANJU XUE[^], MOHAMMED ALNAGGAR[±], GIOVANNI DI
LUZIO[‡] AND GIANLUCA CUSATIS*

* Northwestern University, Civil and Environ. Eng.
Evanston, 60208, IL, USA
e-mail: g-cusatis@northwestern.edu

[†]North Fracture Group
Houghton, MI 49931, USA

[‡] University of New Mexico, Civil, Const. and Environ. Eng.
Albuquerque, NM 87131, USA

[∨] Université de Pau et des Pays de l'Adour, CNRS, LFCR
Allée du Parc Montaury, Anglet, 64600 France

* Virginia Tech, Civil, Civil and Environ. Eng.
103 Patton Hall Blacksburg, VA, USA 24061

* The Hong Kong University of Science and Technology, Dept. of Civil and Environ. Eng.
Clear Water Bay, Hong Kong, 999077, China

[^] Brno Univeristy of Technology, Faculty of Civil Engineering
Brno, 60200, Czechia

[±]Oak Ridge National Laboratory
Oak Ridge, TN 37830, USA

[‡]Politecnico di Milano, Department of Civil and Environ. Eng.
Milan, 20133, Italy

Key words: Lattice discrete particle, heterogeneity, explicit solver, implicit solver, numerical implementation

Abstract. The Lattice Discrete Particle Model (LDPM) is a discrete mesoscale model of concrete that can accurately describe the macroscopic behavior of concrete during elastic, fracturing, softening, and hardening regimes. The LDPM formulation is obtained by modeling the interaction among coarse meso-scale aggregate pieces between polyhedral cells (each containing one aggregate particle) whose external surfaces are defined by sets of triangular facets. At each facet, a vectorial form of constitutive model is used to simulate physical mechanisms such as tensile fracture, cohesion, friction, etc. LDPM has been calibrated and validated extensively through the analysis of a large variety of experimental tests. Numerical results show that it can reproduce with great accuracy the response of concrete under uniaxial and multiaxial stress states in both compression and tension and under both

quasi-static and dynamic loading conditions. In this presentation, we will give an overview of recent implementations of LDPM in various computational platforms. LDPM was implemented in the following software packages: Abaqus/Explicit via user subroutine; Project Chrono, a physics-based modeling and simulation infrastructure based on a platform-independent open-source design; Cast3m a multi-physics software developed by CEA; Open Academic Solver, an open-source software developed at Brno University; JAX-LDPM, an open-source GPU-based software in active development by researchers from the Hong Kong University of Science and Technology; and FE-MultiPhys, developed at Virginia Tech. The different implementations will be compared by simulating typical failure tests for concrete, including, unconfined compression test, three-point bending test, and direct tensile test. Finally, the presentation will provide a vision for future LDPM developments that will likely be implemented in these software packages.

1 INTRODUCTION

Cementitious composites, such as concrete, are widely used in engineering applications. These materials are heterogeneous and exhibit quasi-brittle behavior, with their mechanical response being significantly influenced by phenomena such as crack initiation and propagation, the interaction and coalescence of distributed micro-cracks into a localized macro-crack, the presence of confining pressure, and the crack-bridging effects of fibers. Although traditional continuum mechanics-based models effectively capture global structural responses under some loading conditions, they struggle to simulate material heterogeneity and localized damage under complex loading conditions.

Mesoscale models, which focus on coarse aggregates as individual particles, offer a more efficient alternative to continuum models. Among these, the Lattice Discrete Particle Model (LDPM), developed by Cusatis and coworkers [1], is a significant advancement. LDPM simulates heterogeneous materials at the scale of major heterogeneity, such as coarse aggregate pieces in concrete or grains in rocks [2, 3, 4]. LDPM exhibits superior predictive capabilities in comparison with continuum-based models by inherently incorporating a material length scale based on major material heterogeneity. This enables the accurate simulation of nonlocal effects on strain-softening behavior without introducing numerical artifacts or requiring the computational complexity of gradient-based or integral nonlocal models [5,

6, 7, 8, 9, 10, 11, 12].

Traditionally, LDPM has been numerical implemented using explicit time integration solvers. Specifically, the central difference scheme was successfully adopted in many different studies [13, 14]. It overcomes the convergence challenges typically encountered with implicit algorithms under strain-softening conditions [15]. However, The central difference scheme [16, 17, 18], is conditionally stable which means it is only stable when the time step size is kept below a certain critical value. In standard LDPM simulations, the stable time increment is approximately on the order of 10^{-7} seconds. However, this limits the total simulation time to just a few seconds which makes it impossible to model quasi-static loading scenarios lasting several minutes or sustained loading cases lasting decades. To address this challenge, various workarounds have been proposed, wherein explicit solvers are utilized to simulate at loading rates that exceed the actual loading rate. Results of these kind of simulation can be assumed realistic as long as the ratio between kinetic energy, E_k , and internal energy, W_{int} is less than a threshold in the order of 10^{-3} .

On the other hand, implicit solvers are unconditionally stable and thereby it enables the integration of the response under quasi-static and sustained loading conditions with significantly larger time steps. However, the convergence of the iterative algorithm at some time step might become very slow, or even it can fail, especially in case of a response featuring exces-

sive strain softening response.

The main objective of this study is to provide a comparison of the performance of multiple implicit and explicit solvers implemented in various different software packages to solve the LDPM equations of motion. The comparison is made on the basis of typical tests carried out on concrete samples.

2 GOVERNING EQUATIONS

LDPM adopts rigid body kinematics to define measure of strains at the interface of adjacent polyhedral cells. These strain measures (Equation 1) are computed at the centroid of each facet k through a displacement jump, $[[\mathbf{u}]]_k$ such as,

$$\mathbf{e}_k = \frac{1}{l_k} \mathbf{P}_k \cdot [[\mathbf{u}]]_k \quad (1)$$

where $[[\mathbf{u}]]_k = \mathbf{u}_J + \boldsymbol{\theta}_J \times \mathbf{c}_k^J - \mathbf{u}_I - \boldsymbol{\theta}_I \times \mathbf{c}_k^I$, l_k is the tetrahedron edge length connecting particles I and J . Here \mathbf{u} and $\boldsymbol{\theta}$ denote translational and rotational degrees of freedom. $\mathbf{P}_k = [\mathbf{n}_k \ \mathbf{m}_k \ \mathbf{l}_k]^T$, and \mathbf{n}_k , \mathbf{m}_k and \mathbf{l}_k define the appropriate orthonormal vectors of the local reference system (Fig.1d). The normal vector \mathbf{n}_k is aligned with the straight connection of nodes I and J , the tangential vectors can be chosen arbitrarily. The vector \mathbf{c}_k^I points from the node I to the centroid of the k th facet.

Equilibrium is enforced by the linear and angular momentum balance equations of each polyhedral cell as in Equations (2)

$$\sum_{k \in \mathcal{F}_I} A_k \mathbf{P}_k^T \cdot \mathbf{t}_k + V_I \mathbf{b}_I = \mathbf{M}_u^I \cdot \ddot{\mathbf{u}}_I + \mathbf{M}_\theta^I \cdot \ddot{\boldsymbol{\theta}}_I \quad (2a)$$

$$\sum_{k \in \mathcal{F}_I} A_k \mathbf{c}_k^I \times (\mathbf{P}_k^T \cdot \mathbf{t}_k) + V_I \mathbf{r}_I \times \mathbf{b}_I = \mathbf{I}_u^I \cdot \ddot{\mathbf{u}}_I + \mathbf{I}_\theta^I \cdot \ddot{\boldsymbol{\theta}}_I \quad (2b)$$

where \mathcal{F}_I contains all facets of a polyhedral cell I , $A_k = A_{0k} \mathbf{n}_k \cdot \mathbf{n}_{k0}$ is the projected area of a facet orthogonal to the corresponding tetrahedron edge, \mathbf{n}_{k0} is the true normal to the facet plane, V_I is the cell volume, \mathbf{r}_I is the vector from the particle center to the cell centroid, \mathbf{b}_I

is the external body force, \mathbf{t}_k is the traction vector in local reference system, and \mathbf{M}_u^I , \mathbf{M}_θ^I , \mathbf{I}_u^I , and \mathbf{I}_θ^I are inertia tensors of the cell, respectively.

The LDPM governing equations are then completed by a set of vectorial constitutive equations relating tractions and strains: $\mathbf{t} = \mathbf{T}(\mathbf{e})$. In the elastic regime one has $\mathbf{t} = \mathbf{E} \cdot \mathbf{e}$ where $\mathbf{E} = E_0 \mathbf{diag}(1 \ \alpha \ \alpha)$ where E_0 and α are model parameters known as effective normal modulus and shear-normal coupling parameter. LDPM nonlinear, inelastic constitutive equations (schematically shown in Fig.1e, f) have been successfully formulated and validated for concrete and other quasi-brittle materials in previous works by some of the authors to which interested readers are directed for additional information [15].

3 NUMERICAL IMPLEMENTATIONS

LDPM can be implemented in a traditional finite element codes using a tetrahedral mesh. It uses linear tetrahedral element with rotational and translational degrees of freedom. Each tetrahedron has 12 facets resulting from the domain tessellation process (Fig. 1c). Various existing publications [1, 13, 16] present detailed derivation of the LDPM tetrahedral element stiffness matrix, mass matrix, and force vector, which is omitted here for brevity. All the numerical implementations presented in this paper are based on a Lagrangian formulation under the assumption small displacements, small strains and rotations.

After assemblage of all LDPM tetrahedral elements, the general form of the equations of motion for LDPM systems can be written as

$$\mathbf{M} \cdot \ddot{\mathbf{q}} + \mathbf{F}_{\text{int}}(\mathbf{q}) = \mathbf{F}_{\text{ext}} \quad (3)$$

where \mathbf{M} , \mathbf{F}_{int} , \mathbf{F}_{ext} , and \mathbf{q} denote mass matrix, internal forces, external forces, and vector of degrees of freedom (combined \mathbf{u} and $\boldsymbol{\theta}$), respectively. In the elastic case $\mathbf{F}_{\text{int}} = \mathbf{K} \cdot \mathbf{q}$, where \mathbf{K} is the stiffness matrix. The mass matrix can be consistent [17, 1] or diagonalized, which is obtained by simply retaining the diagonal terms of the consistent mass matrix.

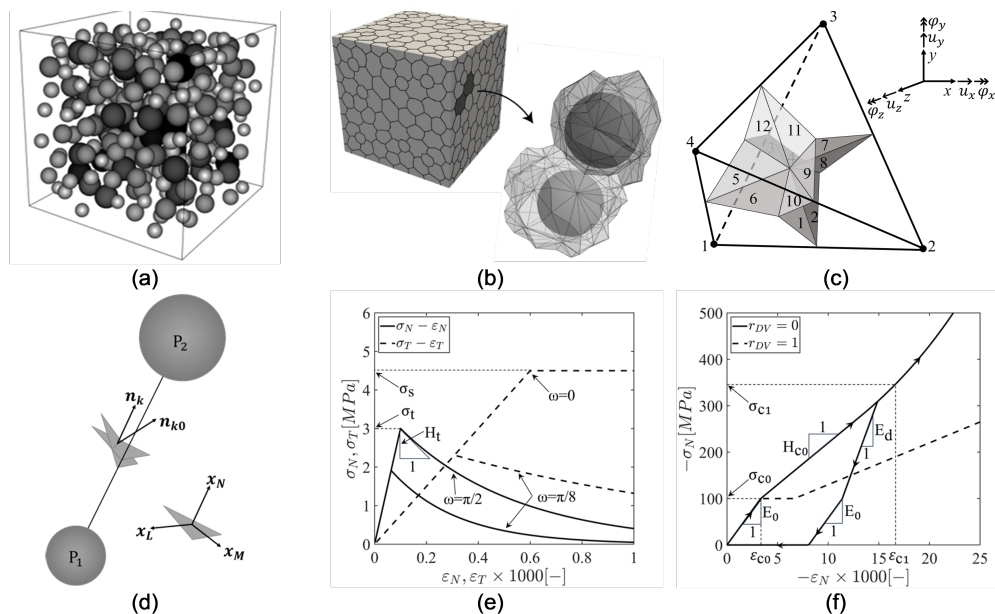


Figure 1: (a) LDPM particles in a cubic geometry following placement procedure; (b) set of two LDPM polyhedral cells composed of a single particle and their surrounding facets; (c) set of four LDPM particles and associated facets; (d) original and projected LDPM facets; (e) typical traction versus strain curves at the LDPM facet level; (f) typical normal traction versus normal strain curves in compression.

3.1 Mesh Generations

All simulations performed in this study relied on the LDPM geometrical input provided by NU-FreeCAD. FreeCAD is an open-source parametric 3D CAD software that is highly suitable for a range of engineering and design tasks. Its integration with Python scripting offers powerful customization and automation capabilities, making it an effective backend tool for developing specialized workflows essential in research and development environments [18]]. Using various Python scripts, the particle placement, meshing, and tessellation procedures described in Ref. [1] were implemented. The output includes LDPM polyhedral cell structures, tetrahedral meshes, and corresponding facet data, which are provided as files that can be read and interpreted by various solvers. The NU-FreeCAD Preprocessor is distributed freely¹ under the BSD 3-Clause License.

¹github.com/Concrete-Chrono-Development/chrono-preprocessor

3.2 Explicit and Implicit Solvers

LDPM is currently implemented in ABAQUS Explicit via a VUEL subroutine [19], Project Chrono [20], JAX [21], Open Academic Solver (OAS) [22], CAST3M [23, 24, 25], FE-MultiPhys [26] and Julia LDPM. The LDPM implementation in these software packages is described in details in Ref. [16]. The same report [16] describes in depth the convergence criteria and convergence threshold adopted in the relevant implicit solvers. In all implicit solvers, the time step size was chosen with the assumption that the number of iterations would typically be less than 50. However, higher number of iterations and possibly also acceptance of non-converging results is allowed in some limited number of time steps. Tab. 1 reports basic information relevant to the adopted solvers.

Table 1: Basic information for the adopted solvers, more information is available in Ref. [16].

ID	Software	Solver Type	Algorithm	Mass Matrix
AE	ABAQUS	Explicit	Central Difference	Lumped
JA	JAX-LDPM	Explicit	Central Difference	Lumped
CI	Chrono	Implicit	HHT	Consistent
OA	OAS	Implicit	Generalized- α	Consistent
CA	CAST3M	Implicit	static	N/A
MP	FEMultiPhys	Implicit	HHT	Lumped
JU	Julia LDPM	Implicit	static, Arc-Length	N/A

4 NUMERICAL RESULTS

4.1 Hardening behavior in uniaxial strain compressive test

First, a uniaxial strain test is simulated. In the numerical analysis, a cylindrical specimen ($D = 100$ mm, $H = 200$ mm) depicted in Figure 2a is subjected to compressive loading. The displacement is applied by increasing velocity progressively increased from 0 to $\dot{u}_z = -5$ mm/s within 0.001 seconds, followed by a constant velocity phase. All degrees of freedom at the bottom nodes, except for rotation around the z -axis, are restricted. Similar constraints are applied to the top surface, but it is free to move in the direction of the applied velocity. Furthermore, lateral displacement is restricted for all nodes along the outer surface of the cylinder.

Figure 2b shows the obtained stress versus strain curves. The general response of test is characterized strain-hardening due to collapse of pores in the concrete material under compression. All the different implementations gives almost identical results as can be seen from the figure. The Fig. 2c illustrates the number of iterations of implicit solvers, all implicit solvers give stable results; however, the OA solver requires an unusually high number of iterations for a single time step. Fig. 2d shows the distribution of the volumetric strain (by CI solver).

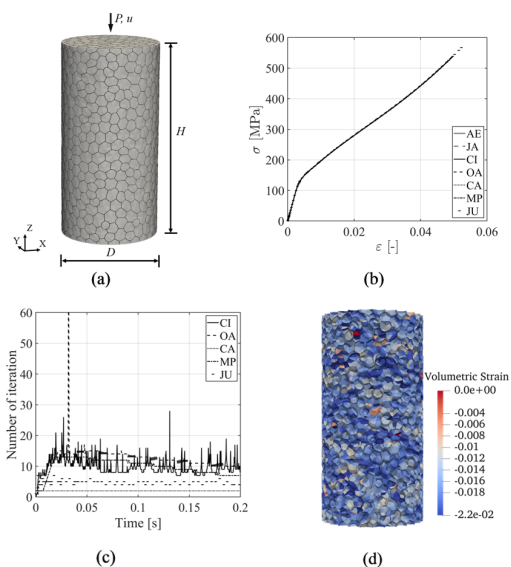


Figure 2: Dimensions of the specimen and obtained simulation results for uniaxial strain test specimens.

The time steps and computational times are reported in Tab. 2 – note that the computational servers and number of threads used for individual runs differ for each software. In this specific example, implicit solvers seem to be more advantageous as they can utilize substantially larger time steps. This efficiency is attributed to the hardening behavior which demands a relatively low number of iterations.

4.2 Fracturing behavior in dog bone tensile test

The next example is a dog bone shaped specimen subjected to direct tension. The specimen is sketched in Fig. 3a, dimensions are $B = H = 150$ mm, $b = D = 50$ mm. All degrees of

Table 2: Time step and total computational time for uniaxial strain test simulation.

	AE	JA	CI	OA	MP	CA	JU
time step [s]	10^{-7}	10^{-7}	10^{-4}	5×10^{-4}	2×10^{-5}	10^{-4}	-
time [h]	2.2	1.6	2.0	0.33	0.67	12.3	2.0

freedom, except rotations around the z-axis, at the bottom surface are constrained. The same boundary conditions are applied to the nodes on the top surface, with the exception of translation along the z-axis. A vertical velocity of $\dot{u}_z = 1 \text{ mm/s}$ is prescribed to the top surface.

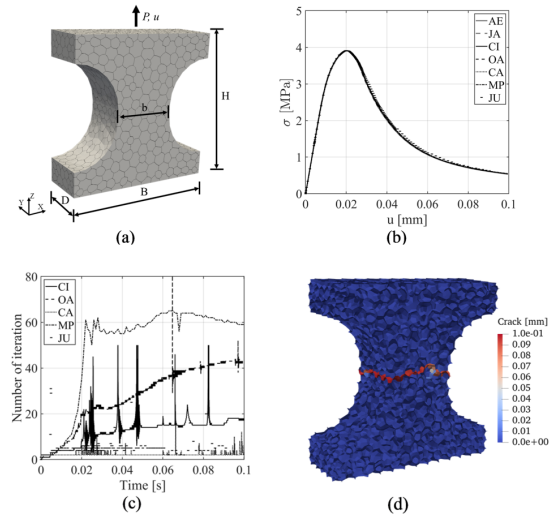


Figure 3: Dimensions of the specimen and obtained simulation results for dog bone tensile test.

The obtained stress-displacement curves are reported in Fig. 3b, stress is related to the central smallest cross-section, $\sigma = P/bD$. Almost all the implementations provide almost identical responses, including the static solvers. The number of iterations throughout the time for implicit solvers is given in Fig. 3c, as can be seen from the figure some of the steps in CI and OA solvers do not converge. The kinetic energy is compared to the internal energy, and its relatively small value indicates that the explicit solvers exhibit stable behavior. Fig. 3d shows crack pattern obtained by CI solver at the end of the simulation. The response is characterized by only one single localized fracture developed in the specimen. The colors in the figure demonstrate total crack opening computed as $\sqrt{w_N^2 + w_M^2 + w_L^2}$ with w_α being the crack openings in local reference system of individual facets.

Table 3 provides time steps and total computational times for individual implementations. The MP solver is the fastest in this case. The computational times for both explicit and implicit solvers are comparable, although the explicit implementations leverage a large number of CPUs or GPUs.

5 CONCLUSIONS

In this study, several LDPM implementations have been compared using benchmarks designed for different loading scenarios. Based on the results obtained in this study, the following conclusions can be drawn.

- Both implicit and explicit solvers can be efficiently used to solve LDPM problems dealing nonlinear material behavior characterized by either strain-hardening or strain-softening.
- It is a misconception that only explicit solvers can handle the LDPM response

Table 3: Time step and total computational time for dog bone tensile test.

	AE	JA	CI	OA	MP	CA	JU
time step [s]	10^{-7}	10^{-7}	2×10^{-5}	2.5×10^{-5}	5×10^{-4}	10^{-4}	-
time [h]	1.33	0.43	3.8	1.67	0.075	4.0	4.1

with excessive nonlinearity and complex crack patterns. However, as the complexity of the strain-softening response increases, implicit solvers tend to be less efficient, primarily due to growing convergence difficulties.

- The choice of solver for computing the LDPM response depends on the specific application. Implicit solvers are more effective for linear response, strain-hardening, or strain-softening with simple crack patterns, while explicit solvers become more advantageous in cases involving complex strain-softening and crack patterns.

Acknowledgement

Jan Eliáš gratefully acknowledges financial support from project INODIN (CZ.02.01.01/00/23_020/0008487) co-funded by European Union. Monika Štředulová acknowledges Brno Ph.D. talent Scholarship funded by the Brno City Municipality.

References

- [1] G. Cusatis, D. Pelessone, and A. Mencarelli. “Lattice discrete particle model (LDPM) for failure behavior of concrete. I: Theory”. In: *Cement and Concrete Composites* 33.9 (2011), pp. 881–890.
- [2] W. Li, R. Rezakhani, C. Jin, X. Zhou, and G. Cusatis. “A multiscale framework for the simulation of the anisotropic mechanical behavior of shale”. In: *International Journal for Numerical and Analytical Methods in Geomechanics* 41.14 (2017), pp. 1494–1522.
- [3] W. Li, X. Zhou, J. W. Carey, L. P. Frash, and G. Cusatis. “Multiphysics lattice discrete particle modeling (M-LDPM) for the simulation of shale fracture permeability”. In: *Rock Mechanics and Rock Engineering* 51.12 (2018), pp. 3963–3981.
- [4] S. E. Ashari, G. Buscarnera, and G. Cusatis. “A lattice discrete particle model for pressure-dependent inelasticity in granular rocks”. In: *International Journal of Rock Mechanics and Mining Sciences* 91 (2017), pp. 49–58.
- [5] Z. P. Bažant. “Nonlocal damage theory based on micromechanics of crack interactions”. In: *Journal of Engineering Mechanics* 120.3 (1994), pp. 593–617.
- [6] J. De Vree, W. Brekelmans, and M. Van Gils. “Comparison of nonlocal approaches in continuum damage mechanics”. In: *Computers & Structures* 55.4 (1995), pp. 581–588.
- [7] G. Di Luzio. “A symmetric over-nonlocal microplane model M4 for fracture in concrete”. In: *International Journal of Solids and Structures* 44.13 (2007), pp. 4418–4441.
- [8] R. H. Peerlings, R. de Borst, W. M. Brekelmans, and J. de Vree. “Gradient enhanced damage for quasi-brittle materials”. In: *International Journal for numerical methods in engineering* 39.19 (1996), pp. 3391–3403.
- [9] G. Pijaudier-Cabot and Z. P. Bažant. “Nonlocal damage theory”. In: *Journal of engineering mechanics* 113.10 (1987), pp. 1512–1533.
- [10] P. Havlásek, P. Grassl, and M. Jirásek. “Analysis of size effect on strength of quasi-brittle materials using integral-type nonlocal models”. In: *Engineering Fracture Mechanics* 157 (2016), pp. 72–85.

- [11] E. Lale, X. Zhou, and G. Cusatis. “Iso-geometric implementation of high-order microplane model for the simulation of high-order elasticity, softening, and localization”. In: *Journal of Applied Mechanics* 84.1 (2017), p. 011005.
- [12] G. Pijaudier-Cabot and J. Khoury. “Damage Mechanics for Quasi-Brittle Materials: Continuum and Lattice Descriptions”. In: *Comprehensive Mechanics of Materials (First Edition)*. Ed. by V. Silberschmidt. First Edition. Oxford: Elsevier, 2024, pp. 303–324. ISBN: 978-0-323-90647-0.
- [13] G. Cusatis, A. Mencarelli, D. Pelessone, and J. Baylot. “Lattice discrete particle model (LDPM) for failure behavior of concrete. II: Calibration and validation”. In: *Cement and Concrete composites* 33.9 (2011), pp. 891–905.
- [14] E. Lale, R. Reza khani, M. Alnagar, and G. Cusatis. “Homogenization coarse graining (HCG) of the lattice discrete particle model (LDPM) for the analysis of reinforced concrete structures”. In: *Engineering Fracture Mechanics* 197 (2018), pp. 259–277.
- [15] C. Ceccato, M. Salviato, C. Pellegrino, and G. Cusatis. “Simulation of concrete failure and fiber reinforced polymer fracture in confined columns with different cross sectional shape”. In: *International Journal of Solids and Structures* 108 (2017), pp. 216–229. ISSN: 0020-7683. URL: <http://www.sciencedirect.com/science/article/pii/S0020768316303900>.
- [16] E. Lale, K. Yu, M. Troemner, J. Eliáš, M. Středulová, T. Xue, I. Koutromanos, B. Ayhan, G. Pijaudier-Cabot, J. Khoury, D. Toussaint, A. Tasora, M. Pathirage, Y. Lyu, M. Alnagar, G. D. Luzio, L. Yang, L. Shen, and G. Cusatis. *On the Computation of the Lattice Discrete Particle model (LDPM) Response with Various Time Integration Solvers*. SPREE INTERNAL REPORT No. 4-3/448O. Department of Civil, Environmental Engineering, Center for Science, and Protection of Engineered Environments (SPREE), Northwestern University, 2024.
- [17] J. S. Archer. “Consistent mass matrix for distributed mass systems”. In: *Journal of the Structural Division* 89.4 (1963), pp. 161–178.
- [18] FreeCAD Community. *FreeCAD Documentation*. 2023. URL: https://www.freecadweb.org/wiki/Main_Page.
- [19] M. A. Troemner. “Multiscale lattice discrete particle modeling of concrete: micromechanics, scaling, dynamics”. PhD thesis. Northwestern University, 2022.
- [20] A. Tasora, R. Serban, H. Mazhar, A. Pazouki, D. Melanz, J. Fleischmann, M. Taylor, H. Sugiyama, and D. Negrut. “Chrono: An open source multiphysics dynamics engine”. In: *High Performance Computing in Science and Engineering: Second International Conference, HPCSE 2015, Soláň, Czech Republic, May 25-28, 2015, Revised Selected Papers 2*. Springer. 2016, pp. 19–49.
- [21] T. Xue, S. Liao, Z. Gan, C. Park, X. Xie, W. K. Liu, and J. Cao. “JAX-FEM: A differentiable GPU-accelerated 3D finite element solver for automatic inverse design and mechanistic data science”. In: *Computer Physics Communications* (2023), p. 108802.
- [22] J. Eliáš and G. Cusatis. “Homogenization of discrete mesoscale model of concrete for coupled mass transport and mechanics by asymptotic expansion”. In: *Journal of the Mechanics and Physics of Solids* 167 (2022), p. 105010. ISSN: 0022-5096.
- [23] P. Verpaux and T. Charass. “Millard., A. 1988: CASTEM 2000: une approche moderne du calcul des structures”. In: *Fouet, JM; Ladev~ ze, P.; Ohayon,*

- R.(eds.) Calcul des structures et intelligence artificielle 2* (), pp. 267–287.
- [24] A. Cibelli, M. Pathirage, G. Cusatis, L. Ferrara, and G. Di Luzio. “A discrete numerical model for the effects of crack healing on the behaviour of ordinary plain concrete: Implementation, calibration, and validation”. In: *Engineering Fracture Mechanics* 263 (2022), p. 108266. ISSN: 0013-7944.
- [25] M. Pathirage, F. Thierry, D. Tong, G. Cusatis, D. Grégoire, and G. Pijaudier-Cabot. “Comparative investigation of dynamic implicit and explicit methods for the Lattice Discrete Particle Model”. In: *Computational Modelling of Concrete and Concrete Structures*. CRC Press, 2022. ISBN: 9781003316404.
- [26] I. Koutromanos. *FE-MultiPhys: A Finite Element Program for Nonlinear Analysis of Continua and Structures*. 2024. URL: <https://www.designsafe-ci.org/data/browser/public/designsafe.storage.published/PRJ-4154/%2FPRJ-4154v3%2FDocumentation%20-%20Tutorials?doi=10.17603/ds2-j5mp-a358>.